



# Laboratory and field assessment of mid-infrared absorption (MIRA) instrument performance for methane and ethane dry mole fractions

Yunsong Liu<sup>1,2</sup>, Natasha L. Miles<sup>1</sup>, Scott J. Richardson<sup>1</sup>, Zachary R. Barkley<sup>1</sup>, David O. Miller<sup>1</sup>, Jonathan Kofler<sup>3,4</sup>, Philip Handley<sup>3,4</sup>, Stephen DeVogel<sup>3,4</sup>, Kenneth J. Davis<sup>1,2</sup>

5 <sup>1</sup>Department of Meteorology and Atmospheric Science, The Pennsylvania State University, University Park, PA, 16802, USA

<sup>2</sup>Earth and Environmental Systems Institute, The Pennsylvania State University, University Park, PA, 16802, USA

<sup>3</sup>Global Monitoring Laboratory, National Oceanic and Atmospheric Administration, Boulder, CO, 80305, USA

<sup>4</sup>Cooperative Institute for Research in Environmental Sciences (CIRES), the University of Colorado Boulder, Boulder, CO, 80309, USA

10 *Correspondence to:* Yunsong Liu ([yzl6376@psu.edu](mailto:yzl6376@psu.edu))

**Abstract.** Concurrent measurements of methane (CH<sub>4</sub>) and ethane (C<sub>2</sub>H<sub>6</sub>) can be used to identify and separate methane sources, as ethane is present in thermogenic sources (e.g., oil and natural gas) but not in biogenic sources (e.g., agriculture). In this study, we evaluated the performance of multiple Aeris MIRA Ultra instruments (Versions 1 and 2) through controlled laboratory tests and tower-based deployments under field conditions. The systems were modified with an external pump, flow control, a Nafion dryer, and a custom-built auxiliary box to automate the system and transmit near real-time data. We determined the best calibration approach for our application, given practical limitations, to be a full calibration cycle (with ambient and high calibration cylinders) about once per day and an ambient calibration cylinder sampled hourly. Measurement uncertainty was assessed, including the uncertainty due to instrument noise as a function of calibration frequency, uncertainty in the water vapor correction, and cylinder assignment uncertainty. Instrument noise was the dominant source of uncertainty for C<sub>2</sub>H<sub>6</sub>, while the water vapor correction dominated the CH<sub>4</sub> uncertainty. For Version 2 systems with hourly calibrations and a Nafion dryer with counterflow, the mean total uncertainty, including both systematic errors and noise, of hourly averages was 0.8 - 3.0 ppb CH<sub>4</sub> and 0.35 - 0.37 ppb C<sub>2</sub>H<sub>6</sub>. Laboratory intercomparisons showed network compatibility within 1.2 ppb CH<sub>4</sub> and 0.23 ppb C<sub>2</sub>H<sub>6</sub>, and a collocated deployment with a NOAA Picarro system agreed within 1.8 ppb CH<sub>4</sub>. Instrument noise varied substantially amongst the instruments, with errors reaching up to 11 ppb CH<sub>4</sub> and 2 ppb C<sub>2</sub>H<sub>6</sub> for hourly means, with similar variability indicated in a 50-h cylinder test. With appropriate engineering and calibration, the Aeris MIRA Ultra shows the capability to measure ethane and methane with sufficient stability to distinguish regional methane emission sources in many field settings.

## 1 Introduction

Methane (CH<sub>4</sub>), the second most abundant human-induced greenhouse gas, has an atmospheric lifetime of approximately twelve years and a global warming potential more than 80 times that of carbon dioxide (CO<sub>2</sub>) over a 20-year period (Myhre et al., 2013). Its global average mole fraction has increased by a factor of 2.7 since the pre-industrial era with the highest annual



35 growth rate of 17 ppb recorded in 2021 – the largest since direct measurements began in 1983 (WMO, 2022). Despite being an effective target for rapid climate change mitigation on decadal time scales, methane sources and sinks remain poorly constrained from local to global scales due to the wide variety of anthropogenic and natural emissions, which often overlap geographically (Saunois et al., 2020).

Methane is generated through different processes, categorized as biogenic (e.g. rice paddies, landfills, sewage and wastewater treatment, and ruminants), thermogenic (e.g. coal, oil and natural gas), and pyrogenic (e.g. incomplete combustion of biomass and other organic materials), all of which have anthropogenic and natural contributions. Saunois et al. (2020) report that 60% of global methane emissions are from anthropogenic activities, and about 35% of anthropogenic emissions are related to the production, transportation, and use of fossil fuels, such as coal, oil, and natural gas. Specifically in the United States (U.S.), the Environmental Protection Agency (EPA) reports that the oil and gas sector contributes to approximately 30% of anthropogenic methane emissions (Collins et al., 2022).

45 Top-down studies utilizing atmospheric measurements over the past decade have demonstrated that methane emissions from the oil and gas sector are significantly larger than EPA inventory estimates (Alvarez et al., 2018; Barkley et al., 2023, 2019, 2021; Caulton et al., 2018; Karion et al., 2015; Robertson et al., 2017). This disagreement requires additional data to better characterize methane emissions from U.S. natural gas operations. Ethane ( $C_2H_6$ ) is the second-most abundant component of natural gas produced by thermogenic processes, after  $CH_4$  (Rella et al., 2015; Schwietzke et al., 2014). In contrast, biogenic methane sources do not co-emit  $C_2H_6$ . Therefore, ethane is used as a tracer for fossil fuel based  $CH_4$  emissions. Measuring both  $CH_4$  and  $C_2H_6$  mixing ratios can provide information to disaggregate sources responsible for measured  $CH_4$  enhancements, especially in regions with co-located thermogenic and biogenic methane sources (e.g. the Denver-Julesburg Basin).

In recent years, commercial laser-based spectrometers have been developed with the capability to measure both  $CH_4$  and  $C_2H_6$  mole fractions at high-temporal resolution (Commane et al., 2023; Defratyka et al., 2021a, b; Roscioli et al., 2015). Commane et al. (2023) reported an intercomparison of three newly developed commercial instruments for  $CH_4$  and  $C_2H_6$  and found that a cavity-enhanced infrared absorption spectrometer from Aerodyne Research Inc. performed best, but is more difficult to deploy to field sites due to its large size, high power consumption, and high level of expertise required for operation. The Picarro G2210-i was able to precisely measure methane but not ethane, consistent with previous results (Defratyka et al., 2021a). The MIRA (mid-infrared absorption) Ultra Leak Detection system from Aeris Technologies, a spectrometer that performed well for both  $CH_4$  and  $C_2H_6$ , with noted difficulties related to water vapor, specific setup requirements, and software problems (Commane et al., 2023).

65 In this paper, we present the first systematic assessment of the Aeris MIRA Ultra for long-term, tower-based network measurements of  $CH_4$  and  $C_2H_6$  dry mole fractions. In Section 2, we describe methods for controlling instrument flow rates, managing water vapor, calibration, and automating the instruments for extended deployments, as well as an approach for estimating the various components of measurement uncertainty. We also describe methods of laboratory tests of multiple Aeris MIRA Ultra instruments and a field comparison at a National Oceanic and Atmospheric Administration (NOAA) site. In



Section 3, we quantify the measurement uncertainty, and calculate the bias and precision from the laboratory and field tests. Finally, we discuss limitations and implications for future applications in Section 4.

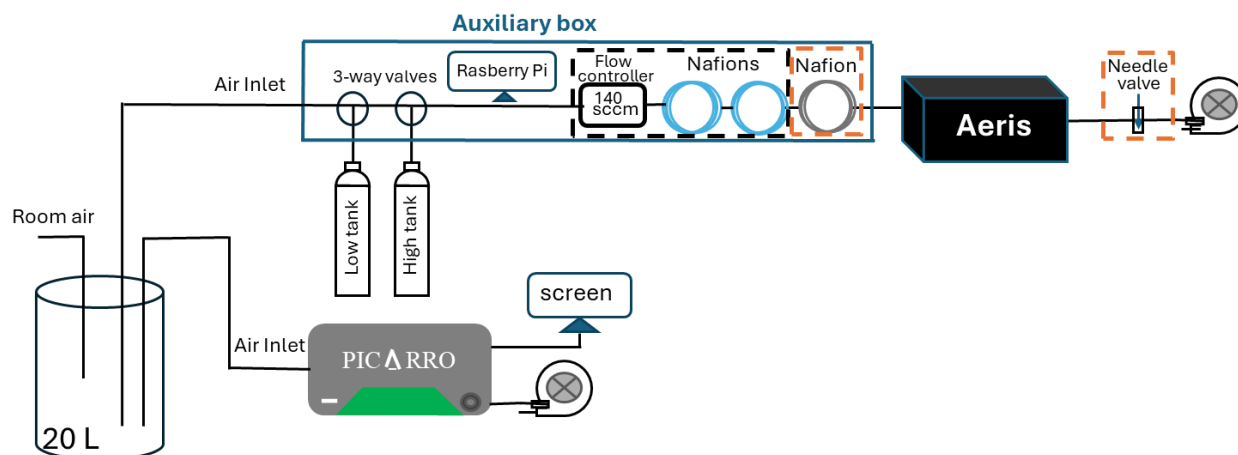
## 2 Methodology

### 2.1 Methane and ethane sensor description

70 To measure methane and ethane dry mole fractions, we use MIRA Ultra mobile mid-infrared laser absorption spectroscopic gas instruments from Aeris Technologies Inc, with modifications detailed in this section. The instruments use a compact, pressure-stabilized (240 mbar) and temperature-stabilized (near 42 °C) sensor core with a 60 cm<sup>3</sup> multi-pass cell. The instrument weighs approximately 9 kg with dimensions of 37 cm×31 cm×18 cm.

As the manufacturer upgraded the configurations for this instrument throughout 2024, we assessed and used two versions of the Aeris MIRA Ultra, eight instruments in total. The original version (Version 1) used a proportional valve downstream of the measurement cell with stainless steel internal tubing. The upgraded version (Version 2) uses an upstream proportional valve with Synflex 1300 internal tubing. The laser is locked to the wavelength of a water vapor absorption peak for Version 1, whereas for Version 2, the laser lock switches to the methane line when the water vapor is below a threshold (about 1000 ppm). This study focuses primarily on the description of laboratory and field tests using the updated Version 2 of the sensor as it is the main version available commercially.

A portable auxiliary box was constructed and placed upstream of each MIRA instrument to facilitate the use of calibration standards and to provide remote data access (Fig. 1). The sample air passes through a pair of three-way valves (Parker, 091-0094-900) that permits the switching of calibration cylinder air into the sample line. A Raspberry Pi (Model 4B) based control system with custom Python operating code controls the three-way valves on a user-defined schedule. As the Aeris reported time is unreliable, the Raspberry Pi performs daily a Network Time Protocol (NTP) synchronization to set the system time. The system also reads the MIRA data stream and combines it with the current time and the three-way valve states. The data files are periodically uploaded to a remote server for processing.



90 **Figure 1: Schematic of the Aeris MIRA Ultra measurement systems for laboratory testing. The components in the black dashed square are included for Version 1 of the Aeris MIRA Ultra and those in the orange dashed square are used for Version 2, while the other components are common to both setups. A total of four identical Aeris systems were measured in parallel for both Version 1 and Version 2 setups.**

Sample water vapor, which was regulated to minimize dependence on the water vapor correction, was controlled differently in the two instrument versions. Relatively high mole fractions of water vapor ( $> 5000$  ppm) were required to keep the spectra  
95 locked on the water line in Version 1 so the typical approach of drying (Andrews et al., 2014) was not possible. To stabilize the water vapor mole fraction and to reduce the dependence on the manufacturer's water correction, we instead minimized the difference of the water vapor mole fractions between the sample air and calibration gases by humidifying the calibration gas  
100 to near ambient water levels using two Nafion tube dryers/water exchangers (Perma Pure LLC: MD-070-96S-2 and MD-070-144S-2) without counterflow (Fig. 1). The use of two different dryers/water exchangers was due to availability; a single longer dryer/water exchanger may have achieved the same result. For Version 2 the software did not require high mole fractions of  
105 water vapor and thus the sample could be dried to below 2000 ppm  $\text{H}_2\text{O}$  using one Nafion tube dryer/water exchanger (Perma Pure Nafion MD-070-144S-2) with counterflow. Typical differences between the dried sample and the humidified calibration gas were 100 - 500 ppm  $\text{H}_2\text{O}$ .

We engineered methods to control the flow rate of the sample gas, with changes reflecting differences in the two versions of  
105 the instrument. The components for Version 1 (Fig. 1) include a mass flow controller set to 140 sccm. The mass flow controller was needed to minimize pressure differences (thought to occur because of the proportional valve being on the outlet rather than the inlet) and to stabilize the water vapor mole fraction when switching between calibration gases and sample air. To simplify field maintenance and minimize the use of calibration gas, the internal pump was disconnected, and an external pump was installed. The flow rate was adjusted from 380 sccm to approximately 140 sccm for laboratory testing and 110 - 140 sccm  
110 for field deployment using a mass flow controller for Version 1. For Version 2, a needle valve was used to adjust the flow rate instead of a mass flow controller (Fig. 1).



## 2.2 Goals for bias and precision of CH<sub>4</sub> and C<sub>2</sub>H<sub>6</sub>

Based on expected signals in the Denver-Julesburg Basin, we set bias (defined as the long-term mean) and precision (defined as the standard deviation of hourly differences) goals of better than 3 ppb CH<sub>4</sub> and 0.3 ppb C<sub>2</sub>H<sub>6</sub>. In general, network compatibility goals are the maximum instrument biases that can be accepted without adversely affecting model interpretation of gradients (GAW Report No. 292, 2022), whereas the total uncertainty contains both bias and random noise. Summertime tower CH<sub>4</sub> enhancements in the Permian Basin averaged around 60 ppb, while wintertime enhancements averaged around 200 ppb (Monteiro et al., 2022). Considering the lower emissions in the Denver-Julesburg Basin, a desire for bias less than 10% of typical network enhancements any time of the year, and instrument capabilities, we set the bias goal to 3 ppb CH<sub>4</sub>. Assuming a 10% CH<sub>4</sub> to C<sub>2</sub>H<sub>6</sub> ratio, the corresponding bias goal for C<sub>2</sub>H<sub>6</sub> is 0.3 ppb. We also set precision goals for the hourly differences (also 3 ppb CH<sub>4</sub> and 0.3 ppb C<sub>2</sub>H<sub>6</sub>) to limit the deviations that may impact emissions from inversion modeling on shorter timescales, e.g., weekly, timescales.

## 2.3 Laboratory tests

Prior to deployment, we conducted a series of laboratory tests (Tests 1, 2, and 3 in Table 1) to assess the accuracy, precision, and stability of the instruments, to characterize the water vapor response, and to calibrate the field cylinders for C<sub>2</sub>H<sub>6</sub>. We summarize the methods for these tests below.

**Table 1: A summary of the laboratory and field tests.**

Test number	Test description	Instrument serial number	Instrument version	Analysis
<b>Test 1: Multi-hour cylinder test with nafion</b>	12 h cylinder tests with nafion.	A665, A792, A800, A886	Version 2	<b>Water vapor uncertainty:</b> Determine water vapor correction if possible and estimate component of uncertainty, U <sub>w</sub> .
				<b>Allan deviation:</b> Use time period with low and stable water vapor calculate Allan deviation to 1) compare performance between instruments, 2) determine optimal averaging time, and 3) inform needed frequency for calibration.
<b>Test 2: Multi-hour cylinder test</b>	50 h cylinder test (no Nafion).	A792	Version 2	<b>Uncertainty due to instrument noise:</b> Determine needed frequency for calibration. Estimate component of uncertainty due to drift between calibration cycles, U <sub>n</sub> .
<b>Test 3: Multi-cylinder testing</b>	Cycle through 3 NOAA tertiary tanks and each of 17 cylinders treated as unknowns, repeated 16-32 times for each unknown cylinder.	A792	Version 1	<b>Cylinder calibration:</b> Calibrate the unknown cylinders for C <sub>2</sub> H <sub>6</sub> . Quantify repeatability as standard deviation of the calibration cycles.
	CH <sub>4</sub> is known for all tanks based on calibrations with Picarro instrument. C <sub>2</sub> H <sub>6</sub> is known for 6 of the cylinders from NOAA.			<b>Determine C<sub>2</sub>H<sub>6</sub> cylinder assignment uncertainty.</b> Estimate component of C <sub>2</sub> H <sub>6</sub> uncertainty, U <sub>c</sub> , due to cylinder assignment errors by comparing to NOAA values.
<b>Test 4: Concurrent laboratory test</b>	Concurrent lab test sampling room air with two calibration cylinders for each system. Concurrent Picarro CH <sub>4</sub> measurements.	A665, A792, A800, A886	Version 1 (8 h) and Version 2 (10 days)	<b>Concurrent lab test.</b> Calculate mean bias and standard deviation of hourly calibrated values for CH <sub>4</sub> and C <sub>2</sub> H <sub>6</sub> . Compare to total uncertainty, U <sub>t</sub> . Test calibration approach using both high and ambient cylinders every hour compared using high cylinder every 25 hours and ambient cylinder every hour.
	Drop power for 10 s and for 12 h.			<b>Warm-up test.</b> Determine necessary length of warm-up time for field measurements by examining calibration gas response.
<b>Test 5: Field test</b>	Co-location at NOAA CAO tower (CH <sub>4</sub> ).	A778, A665	Version 1 and Version 2	<b>Field test.</b> Calculate mean bias and standard deviation of hourly calibrated values for CH <sub>4</sub> . Compare to total uncertainty, U <sub>t</sub> .



### 130 **2.3.1 Multi-hour cylinder tests (Tests 1 and 2)**

We tested the manufacturer's water vapor correction of four instruments by sampling a cylinder filled with dry air passing through a humidified Nafion water exchanger (Test 1). Prior to the water vapor dependence test, the membrane inside the Nafion water exchanger was humidified using room air. Then air from a calibrated cylinder with well-known methane and ethane was pulled through the inner tube of the humidified Nafion water exchanger, such that air from the cylinder was  
135 humidified to about 0.8% by volume initially and gradually dried to about 0.02% over about 12 h. If the water correction was perfect, the reported CH<sub>4</sub> and C<sub>2</sub>H<sub>6</sub> dry mole fractions would not depend on the water vapor level of the resulting air. We performed this test with four instruments (serial numbers A665, A792, A800 and A886, all Version 2 instruments). We used this data to estimate the uncertainty due to an imperfect water vapor correction (method described in Section 2.4.1).

We used the same data (Test 1) to compare the noise levels amongst the instruments, to determine the optimal averaging time  
140 for calibration cycles, and to inform the needed frequency of calibration by calculating the Allan deviation as a function of averaging time (Allan, 1987; Filges et al., 2015; Shah et al., 2019). To partially separate the effects of instrument noise from variations due to water vapor, we used only the last two hours of data from Test 1 with relatively low and stable water vapor (250 - 350 ppm H<sub>2</sub>O) for these calculations.

To assess the drift of the instruments between calibration cycles, we sampled a cylinder of near ambient values of methane  
145 and ethane for a period of just over two days (50 h) using instrument serial number A792 (Test 2). Instrument A792 was selected for this test because its Allan deviation is representative of the group (i.e., neither the lowest nor the highest; see Section 3.2). The exact dry mole fractions for CH<sub>4</sub> and C<sub>2</sub>H<sub>6</sub> of this cylinder were not available, and are not important as we only need a constant sample to assess the drift of the baseline calibration. The cylinder gas was sampled directly so the water was nearly zero. While the Allan deviation (Test 1) is used to determine the periods at which instrument drift becomes  
150 important, it does not quantify the error caused by the drift between calibration cycles. We used data from Test 2 to determine the noise component of uncertainty as a function of calibration frequency (as described in Section 2.4.2).

### **2.3.2 Field cylinder C<sub>2</sub>H<sub>6</sub> calibrations (Test 3)**

For calibrations of field cylinders with unknown C<sub>2</sub>H<sub>6</sub> dry mole fractions, we used one Aeris MIRA Ultra instrument (serial  
155 number A778, Version 1) to measure the methane and ethane values of each cylinder (Test 3). We calibrated the Aeris instrument using three NOAA tertiary standards calibrated for methane (1985.9 to 2284.7 ppb) and ethane (1.3 to 22.9 ppb) by the Central Calibration Laboratory (CCL) at the National Oceanic and Atmospheric Administration (NOAA) Global Monitoring Laboratory (GML). The CCL maintains the World Meteorological Organization (WMO) methane scale (WMO X2004A) and an internal CCL standard for ethane (C<sub>2</sub>H<sub>6</sub>-2012). Several calibration cycles, sampling the NOAA-calibrated  
160 tertiaries and the field cylinders in turn, were necessary to average the instrument noise and to determine the repeatability of the calibration values. Of the 17 field cylinders, 11 had unknown C<sub>2</sub>H<sub>6</sub> mole fractions, and 6 were calibrated by NOAA CCL but treated as unknown. Each calibration cycle included 4 min for each calibrated and unknown gas (totaling 16 min), with the



remainder of the half hour (14 min) sampling room air. Including periods sampling relatively humid room air was necessary as the laser lock was lost if (very dry) calibration cylinders were sampled for an extended period for the Version 1 instruments. Using valves to automate the sequence, the test was repeated for about 8-16 h per field cylinder. The calibration results for the cylinders exhibited instability for several hours before stabilizing. The initial instability occurred for all cylinders and the cause is unknown. We included all the calibration cycles in the calculation of the cylinder statistics. The field cylinders were calibrated for CH<sub>4</sub> using the method utilized in Richardson et al. (2017). We used data from Test 3 to estimate the uncertainty in the assignment of C<sub>2</sub>H<sub>6</sub> for the field cylinders (Section 2.4.3).

## 2.4 Uncertainty estimation

The uncertainty of the field observations is a combination of errors in the water correction, drift between calibration cycles (instrument noise), and errors in the mole fractions assigned to each field cylinder (cylinder assignment error). Other factors such as equilibration after gas switching, nonlinearity of the true calibration curve, and changes in the calibration slope on time scales shorter than the time between full calibration cycles (tested in Section 3.6.1) are assumed to be small and not included in the uncertainty estimate. We use Tests 1, 2, and 3 (Table 1) to estimate the uncertainty.

### 2.4.1 Uncertainty due to imperfect water corrections

We used data from multi-hour cylinder tests (Test 1) to estimate the uncertainty attributable to imperfect water corrections provided by the manufacturer, despite difficulties in separating water vapor effects from instrument noise. In the field, if the calibration cylinder could be humidified to match the water vapor of the dried sample air, the effect of water vapor on the dry mole fractions would be removed by calibration. In practice, there is a difference between the water vapor during calibration cycles and the sample and this difference changes depending on atmospheric humidity and temperature. Using data from Test 1, we determined the slope of the difference between measured and known CH<sub>4</sub> and C<sub>2</sub>H<sub>6</sub> dry mole fractions as a function of water vapor for each instrument. The slope for the instrument most sensitive to water vapor (serial number A665) represents an upper bound on the error caused by imperfect water corrections for a given water vapor difference. As an estimate of the uncertainty due to water vapor,  $U_w$ , we multiplied the measured water vapor difference in the field at each site as a function of time by this slope.

### 2.4.2 Uncertainty due to instrument noise

We used data from Test 2 to estimate the uncertainty caused by stochastic drift (instrument noise) in the measurements of Aeris instruments between offset (single cylinder) calibration cycles as a function of calibration frequency. We use the term “stochastic” drift to differentiate the instrument behavior from deterministic drift. Stochastic drift is not random, but does decrease as the averaging time is increased. In the field, the drift between calibration cycles is unknown, but here we simulated offset calibration cycles by continuously sampling from a cylinder for 50 h (Test 2). In the obviously unrealistic case that we calibrate continuously, the error due to drift is zero. We computed two-minute means to mimic the time scale of the calibration



cycles in the field. We then simulated calibration cycles by selecting points separated by a range of possible periods between cycles (15 min up to 25 h). We then applied an offset correction, linearly interpolating between the simulated calibration cycles. 195 The error due to instrument drift is the difference between this applied offset calibration between calibration points and the (measured) true behavior of the instrument. We estimate the uncertainty due to instrument noise as the standard deviation of these differences. For reporting the uncertainty in the calibrated dataset, we used these estimates of the instrument noise uncertainty,  $U_n$ , with this estimate changing in time as it depends on the calibration frequency used.

### 2.4.3 Cylinder assignment uncertainty

200 Our estimate of the cylinder assignment uncertainty ( $U_c$ ) is based on the uncertainty of the tertiary cylinders used to calibrate the field cylinders and uncertainty of the scale transfer using the Picarro instrument for  $\text{CH}_4$  and the Aeris for  $\text{C}_2\text{H}_6$ . The tertiary cylinder uncertainty assigned by NOAA (<https://gml.noaa.gov/ccl/refgas.html>, last access: 6 October 2025) was 0.1 ppb  $\text{CH}_4$ . Considering also the uncertainty of the scale transfer, we estimate the cylinder assignment uncertainty for methane based on calibrations using a Picarro instrument to be 0.3  $\text{CH}_4$  based on WMO/IAEA Round Robin Comparison Experiment results 205 (personal communication, NOAA GML). For  $\text{C}_2\text{H}_6$ , we estimate the cylinder assignment error based on the root mean square of the values of the differences between the Penn State and NOAA calibration values (Section 3.4).

### 2.4.4 Total uncertainty

We take the square root of the squared uncertainty components to determine the quadrature sum of the total uncertainty (Eq. 1)

$$210 \quad U_t = \sqrt{U_n^2 + U_w^2 + U_c^2} \quad (\text{Equation 1})$$

where  $U_t$  is the total uncertainty,  $U_n$  is the uncertainty due to the instrument noise,  $U_w$  is the uncertainty of the water correction, and  $U_c$  is the uncertainty in the field cylinder dry mole fractions.

## 2.5 Laboratory and field comparisons

We compared the bias and the precision of calibrated hourly dry mole fractions during concurrent laboratory tests (Test 4) and 215 during a field deployment at NOAA's Colorado Atmospheric Observatory (CAO) (Test 5) to our target compatibility and to the estimated uncertainty.

### 2.5.1 Concurrent laboratory tests (Test 4)

To quantify the measurement bias of individual instruments as a proxy for intra-network compatibility, we conducted concurrent measurements (Test 4) with four Version 2 Aeris instruments and a Picarro Inc. (model G2301) cavity ring-down spectroscopy (CRDS) instrument (Fig. 1). Picarro instruments are the standard widely used for greenhouse gas monitoring 220 networks (e.g., Yver Kwok et al., 2015). The air inlets for both the Picarro and Aeris MIRA Ultra sampled from an actively-

mixed 20 L stainless steel mixing volume. The sampled methane and ethane varied from 2030 - 2378 ppb CH<sub>4</sub> and 0.3 - 13.0 ppb C<sub>2</sub>H<sub>6</sub> in the laboratory during this 10-day (15-25 November 2024) test.

Two high-pressure calibration standard gas cylinders with known concentrations of CH<sub>4</sub> and C<sub>2</sub>H<sub>6</sub> were used to calibrate each  
225 Aeris system. We conducted calibration cycles (i.e., measured both ambient and high cylinders - which we refer to as a full calibration cycle) every 3 h. To ensure stabilization after adequately flushing the cell of the instrument, each standard gas was sampled for 4 min continuously, with only the last 2 min of data used to calibrate the instrument using a linear fit.

We compared the hourly calibrated dry mole fractions amongst the four instruments. The mean methane bias, defined as the long-term average of hourly difference between each of the Aeris instruments and the Picarro instrument, was calculated, as  
230 well as the standard deviation of the hourly differences. Since no reference instrument was available for ethane, the mean ethane bias and standard deviation was calculated between each instrument and the mean ethane value derived from the four instruments. Similar tests were performed for four Version 1 Aeris instruments for a period of 8 h. To check if the deviations can be reduced by averaging, we computed biases and standard deviation as a function of averaging time using the ten-day dataset.

235 **Alternative calibration approach:** In the data processing, we tested an alternative calibration approach in which we used one full calibration cycle at the beginning of the test, but ignored the subsequent high cylinder results. Following the initial full calibration, we adjusted only the offset using the ambient cylinder every 3 h.

**Warm-up tests:** As part of the concurrent laboratory tests, we performed warm-up tests to characterize the time needed for the instrument to stabilize after a power loss, assessed based on the measurements of the calibration gases. We intentionally  
240 interrupted power to all four systems for 10 s by temporarily disconnecting them. Additionally, the instruments were also shut down for 12 h in order to test a completely cold startup.

### 2.5.2 Field deployment comparison (Test 5)

After laboratory testing, four Aeris MIRA Ultra measurement systems based on Version 1 were deployed in May 2024 forming a tower-based observation network surrounding the Denver-Julesburg Basin (<https://sites.psu.edu/saber/>, last access: 6 October  
245 2025), a region characterized by methane emissions from both the production of oil and gas and animal agriculture. Four Version 1 instruments were initially deployed at CSU, HUC, JLC, and CAO (Fig. 2). Version 1 instruments were replaced by Version 2 instruments in early 2025.

**Set-up:** The NOAA tower site CAO (39.9239° N, 103.9721° W) was chosen for a field comparison with NOAA Picarro CH<sub>4</sub> measurements to assess the bias compared to the calculated total uncertainty. Methane and ethane data from the CAO Aeris  
250 MIRA Ultra were collected starting in June 2024. The tower-based network and the diagram of the field tower setup at CAO is shown in Fig. 2. The NOAA Picarro switched inlet heights (30 m, 100 m, and 479 m AGL) every 5 min with a calibration and sampling protocol based on Andrews et al., (2014). Continuous ethane measurements are not available from the NOAA in situ instrument and flask ethane measurements are collected only at 478 m AGL and thus were not considered for comparison. The NOAA Picarro line was flushed with an additional pump with a high flow rate such that the sample air takes

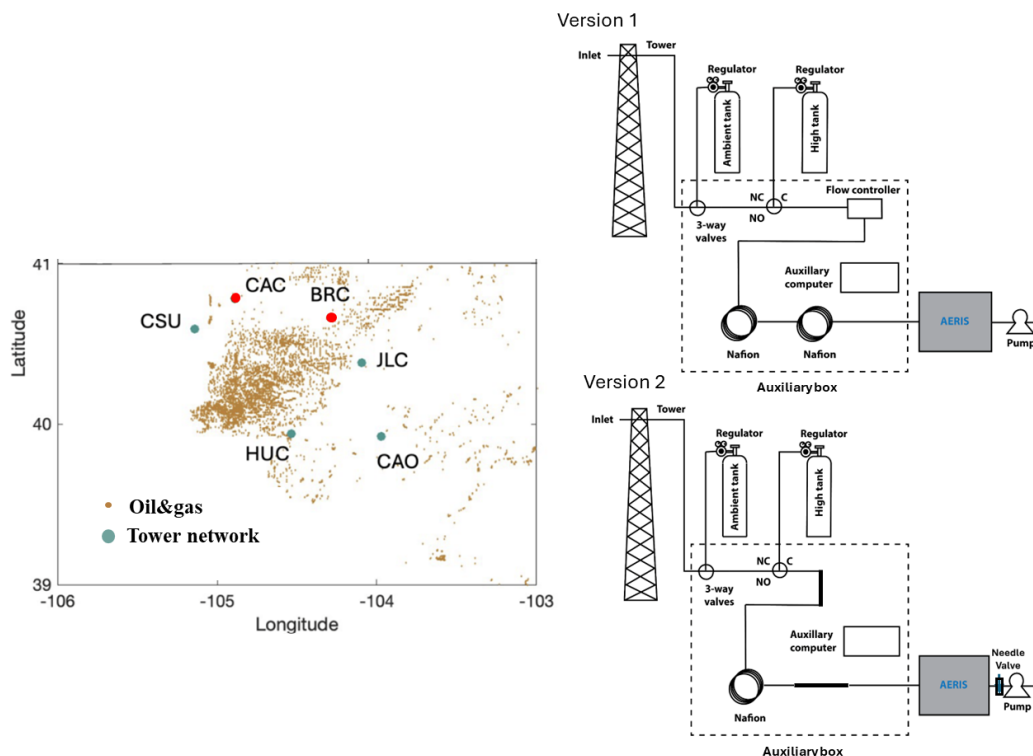


255 only several seconds (8 - 14 s) to reach the instrument and the data were reported as 2-min means every 15 min. The Aeris instrument analyzed air from 30 m AGL using a dedicated sampling line. The flow rate for the Aeris was controlled at 110 sccm, using only the pump for the instrument. With this flow rate, the air took about 20 min to travel from the inlet to the Aeris MIRA Ultra. The timing difference was accounted for in the comparison. To minimize noise that might be caused by mismatches in timing, the hours with large atmospheric variability were removed. We defined “large” as times during which

260 Aeris’ hourly standard deviation or NOAA Picarro’s standard deviation was greater than the 50th percentile. This procedure is only applied for the comparison with the NOAA Picarro at CAO. For all field data, we ignored 3 h of data after a loss of power or other restart to allow for the instrument to fully warm up, despite no obvious indicators of problems (Section 3.6.1).

**Calibration frequency changes:** The calibration frequency for the Aeris instrument changed throughout the deployment, as the optimal procedure was not determined prior to deployment. For 1 June 2024 - 31 December 2024, a full calibration cycle

265 (with ambient and high calibration cylinders) was applied every 3 h. For 7 January 2025 - 8 June 2025, a full calibration cycle was applied every 25 h with an ambient calibration cylinder sampled every 5 h. From 9 June 2025 to the present, a full calibration cycle (with ambient and high calibration cylinders) was sampled about once per day (every 25 h), with an ambient calibration cylinder sampled hourly. We linearly interpolate between hourly offset calibrations.



270 **Figure 2: The tower-based network (left panel) and the diagram of the equipment at the tower sites. Sites CAC and BRC have not yet been deployed. The tower sites were upgraded from Version 1 to Version 2 in early 2025.**



### 3 Results

#### 3.1 Water vapor dependence (Test 1)

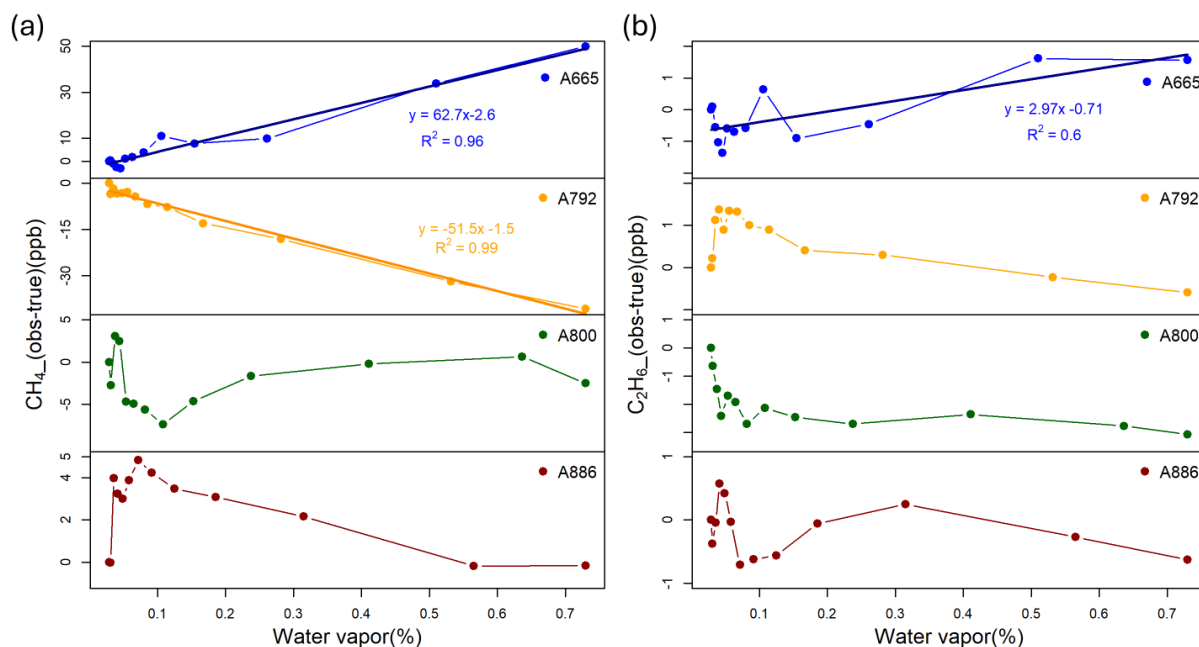
##### 3.1.1 Errors as a function of water vapor

275 The Aeris instruments, using the manufacturer-supplied water vapor correction, showed substantial sensitivity to water vapor  
for measurements of methane and this sensitivity was not consistent between individual instruments. Methane varied by more  
than 50 ppb for serial numbers A665 and A792, and by about 5-10 ppb for A800 and A886 across water vapor levels from  
0.02% to 0.8% (Fig. 4a), indicating better manufacturer water corrections for A800 and A886. Only A665 and A792 showed  
linear responses to changes in water vapor mole fraction (Fig. 4a). Testing the application of these linear water vapor  
280 corrections to the concurrent measurement test (Test 4, Section 3.6.1) from 15-25 November 2024 improved the mean biases  
(between Aeris and Picarro) a moderate amount (from 1.2 to -0.3 ppb CH<sub>4</sub> for A665 and from -1.1 to -0.7 ppb CH<sub>4</sub> for A792).  
Because of instrument noise and lack of repeated tests, we did not apply these potential water vapor corrections to the  
laboratory or field data.

The sensitivity of the ethane measurements to water vapor concentration was not clear, possibly because of instrument drift  
285 during the experiment. Across water vapor levels from 0.02% to 0.8%, ethane errors ranged from -2.8 to 1.6 ppb. Only the  
result for serial number A665 indicated a trend with R<sup>2</sup> greater than 0.5. The instrument drift appeared to be larger in magnitude  
for very low water vapor (less than 0.1%).

##### 3.1.2 Uncertainty due to errors in the water vapor correction

The slope of the instrument exhibiting the largest water vapor dependence (serial number A665 in Fig. 3) is 62.7 ppb CH<sub>4</sub> / %  
290 H<sub>2</sub>O and 2.97 ppb C<sub>2</sub>H<sub>6</sub> / % H<sub>2</sub>O. At typical H<sub>2</sub>O differences of water vapor between the sample and calibration gas of 100-  
500 ppm, depending on site, this corresponds to 0.03-0.15 ppb C<sub>2</sub>H<sub>6</sub> and 0.6-3.0 ppb CH<sub>4</sub>. The error due to water vapor is  
likely a bias that is instrument specific, but it is possible that it changes in time. For ethane, it is possible that the errors in Fig.  
3b result from instrument noise rather than water vapor effects, but the assigned uncertainty is an effort to capture the range of  
the possible effect.



295

300

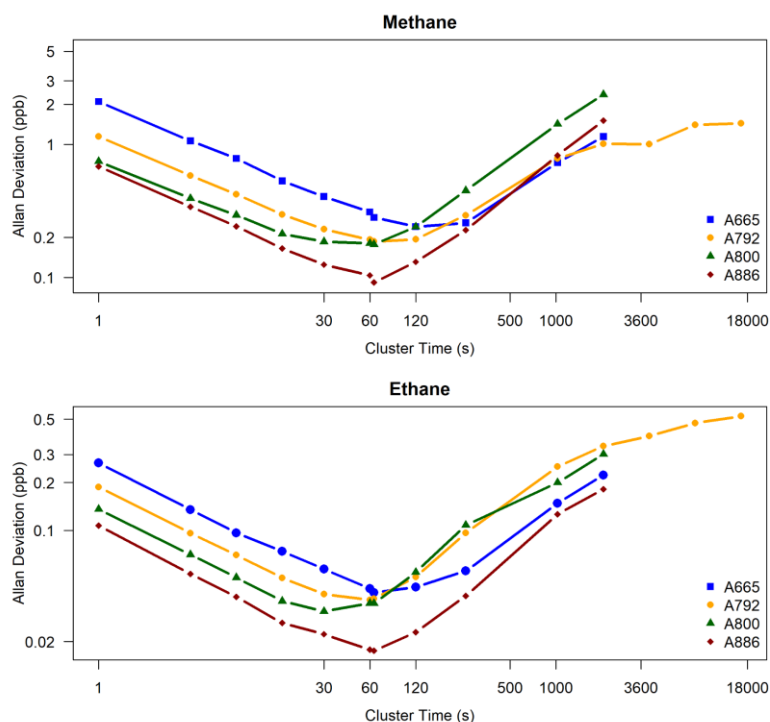
**Figure 3: Water vapor dependence laboratory test for methane (a) of the four instruments (the points represent hourly averaged data), with the y-axis indicating pre-calibration measured compared to known CH<sub>4</sub> values. Water vapor dependence laboratory test for ethane (b) of the four Version 2 instruments. The points represent hourly averaged data. Note that without applying any zero or span using the Aeris software, the errors were up to 190 ppb CH<sub>4</sub> and 15 ppb C<sub>2</sub>H<sub>6</sub>. The data were thus “zeroed” by setting the error at the lowest water vapor value to zero.**

### 3.2 Allan deviation test (Test 1)

In the calculated Allan deviations of the instruments, there are significant differences in performance amongst the instruments for both CH<sub>4</sub> and C<sub>2</sub>H<sub>6</sub>, with the observed precision at 1 Hz ranging from 0.7 ppb to 2.1 ppb for methane and from 0.1 ppb to 0.3 ppb for ethane across the four Version 2 instruments (Fig. 4). The Allan deviation was minimized (precision of 0.1 - 0.3 ppb CH<sub>4</sub> and 0.02 - 0.04 ppb C<sub>2</sub>H<sub>6</sub>, depending on instrument) for averaging times 30 s to 2 min, the optimal averaging time for calibration cycles.

For periods larger than the Allan deviation minimum period, the measurements were affected by drift, suggesting a benefit to calibrating at these timescales, particularly for ethane. For methane, the Allan deviation was less than 1.4 ppb for periods up to 5 h (18000 s), so the drift at this timescale is not significant. For ethane however, the Allan deviation exceeded 0.2 ppb for 17 min (about 1000 s) averaging period and continued to increase (Fig. 4), suggesting a benefit in reducing instrument noise by using a calibration frequency of around 15 min or less, which is unfortunately not practical.

310



315 **Figure 4: The results of Allan deviation tests for four Version 2 instruments. Cylinders with dry mole fractions of about 1980 ppb CH<sub>4</sub> and 1 ppb C<sub>2</sub>H<sub>6</sub> were sampled for 12 h with an inline humidified Nafion dryer/gas exchanger. Only the last 2 h, when the water vapor was relatively low and stable (250-350 ppm H<sub>2</sub>O), was used for this Allan deviation test. Blue, orange, dark green and dark red points are the Allan deviations corresponding to the cluster time, respectively for instrument serial numbers A665, A792, A800 and A886. For serial number A792, the results for the longer Test 2 (without Nafion) are shown, but the results up to 5 min (300 s) are similar for Test 1.**

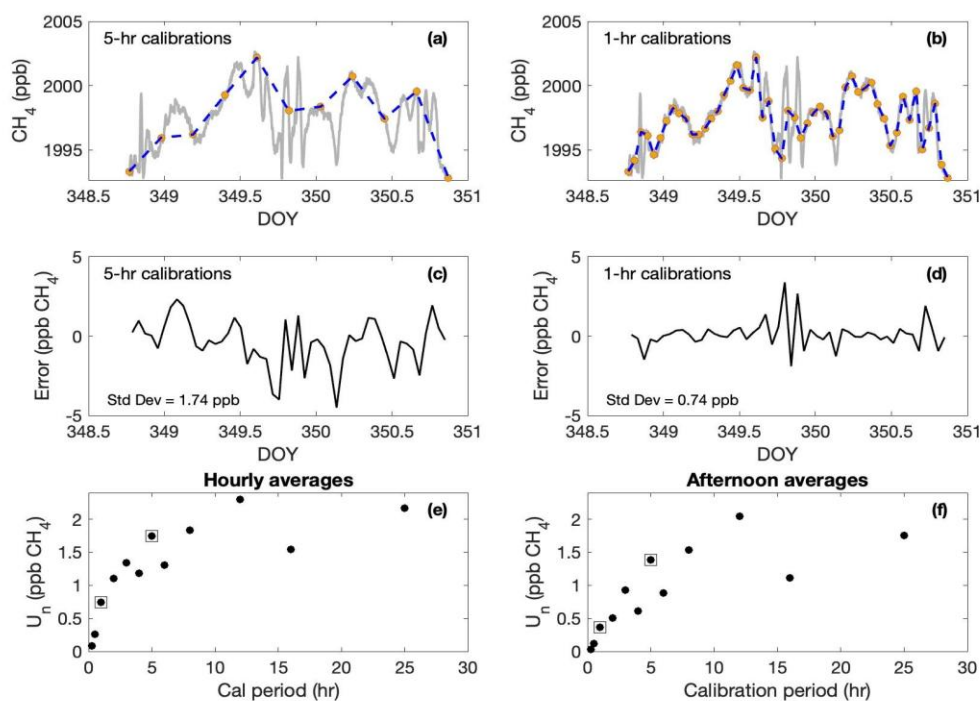
### 3.3 Uncertainty due to instrument noise as a function of calibration frequency (Test 2)

320 The errors due to uncorrected stochastic drift (instrument noise) between calibration cycles are a function of calibration cycle frequency (Figs. 5 and 6). The measured CH<sub>4</sub> and C<sub>2</sub>H<sub>6</sub> would not have a trend between calibration cycles if the instrument did not drift. Instead, the methane varied between 1993 and 2003 ppb CH<sub>4</sub> and the ethane between 1 and 4.5 ppb C<sub>2</sub>H<sub>6</sub> throughout the test (Figs. 5ab and 6ab). The error due to interpolation between 5-hourly calibration cycles is up to ± 4.5 ppb for methane (Fig. 5c) (target compatibility of ± 3 ppb) and ± 1.5 ppb for ethane (Fig. 6c) (target compatibility of ± 0.3 ppb).  
 325 Thus, the variations of ethane between calibration cycles are almost an order of magnitude larger than the target compatibility. While some periods are relatively stable, others exhibit drift as large as 2 ppb C<sub>2</sub>H<sub>6</sub> per hour, necessitating linear interpolation between calibration cycles.

The uncertainty due to noise for ethane is more dependent on the calibration period than for methane, relative to the target compatibility for each species. For example, for calibration cycles separated by 5 h rather than 1 h the uncertainty in the C<sub>2</sub>H<sub>6</sub> increases from 0.25 ppb to 0.49 ppb (Fig. 5e). The uncertainty in the CH<sub>4</sub> is less likely to exceed the target compatibility, as it  
 330 increased from 0.74 ppb (1 h calibration) to 1.74 ppb (5 h calibration) (Fig. 6e). The instrument noise averages out as more



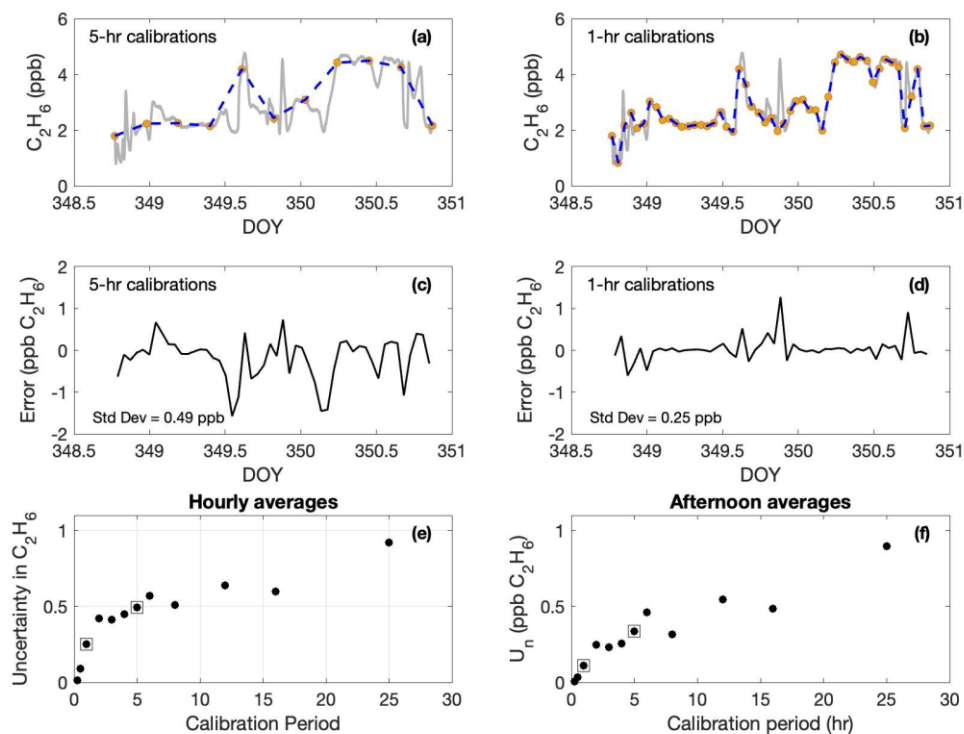
data is considered, so the uncertainty due to noise for afternoon averages (Fig. 5f and Fig. 6f), for example, is less than that of the hourly values (0.37 ppb CH<sub>4</sub> and 0.11 ppb C<sub>2</sub>H<sub>6</sub>). The noise is not completely random, however, as it decreases by less than the square root of the number of data points.



335

340

**Figure 5:** (a-b) Time series of 2-min means of methane (CH<sub>4</sub>) (gray line) during a two-day test sampling a cylinder (with essentially no water) for instrument serial number A792. Colored dots indicate examples of (a) 5-hourly and (b) hourly calibrations. Blue dashed lines indicate linear interpolation between the simulated calibration points. (c-d) Difference between linear interpolation of (c) 5-hourly and (d) 1-hourly calibration cycles and the actual values. This difference is the error associated with stochastic drift between calibration cycles. The standard deviation of these values (averaged over various values for the beginning point) is indicated. (e) Estimated uncertainty attributable to instrument noise as a function of calibration period for hourly means. (f) Same as (e) but for afternoon (5-hourly) means. Calibration periods of 1 h and 5 h are highlighted with squares in (e) and (f).



345 **Figure 6:** (a-b) Time series of 2-min means of ethane ( $C_2H_6$ ) (gray line) during a two-day test sampling a cylinder (with essentially  
 no water) for instrument serial number A792. Colored dots indicate examples of (a) 5-hourly and (b) 1-hourly calibrations. Blue  
 dashed lines indicate linear interpolation between the simulated calibration points. Difference between linear interpolation of (c) 5-  
 hourly and (d) 1-hourly calibration cycles and the actual values. This difference is the error associated with stochastic drift between  
 calibration cycles. The standard deviation of these values is indicated. (e) Estimated uncertainty attributable to instrument noise as  
 a function of calibration period for hourly means. (f) Same as (e) but for afternoon (5-hourly) means. Calibration periods of 1 h and  
 350 5 h are highlighted with squares in (e) and (f).

### 3.4 Cylinder calibrations and assignment uncertainty (Test 3)

The Aeris MIRA Ultra field cylinder calibrations were between 0.01 and 0.19 ppb  $C_2H_6$  different in magnitude compared to NOAA values (Table 2). The root mean square of these differences was 0.12 ppb  $C_2H_6$ , the field cylinder assignment uncertainty.

355 **Table 2:** Comparison of the result of the cylinders measured by Aeris MIRA Ultra (Test 3) and NOAA CCL (all in ppb) for the  
 subset of field calibration cylinders with available NOAA  $C_2H_6$  calibrations. Aeris MIRA Ultra (serial number A778) results include  
 the mean value  $\pm$  standard deviation of the calibration cycles (more than 10 cycles were conducted for each cylinder). Diff\_  $C_2H_6$  is  
 the difference between NOAA calibrated values and the Aeris results.



Cylinder No.	NOAA C <sub>2</sub> H <sub>6</sub>	Aeris MIRA C <sub>2</sub> H <sub>6</sub>	Diff_ C <sub>2</sub> H <sub>6</sub>
CC106646	9.8	9.73±0.07	-0.07
CA02237	24.4	24.22±0.08	-0.18
CB10959	24.7	24.51±0.06	-0.19
CC1801	1.3	1.29±0.04	-0.01
CA02187	1.1	1.13±0.09	0.03
CA03222	1.1	1.19±0.11	0.09

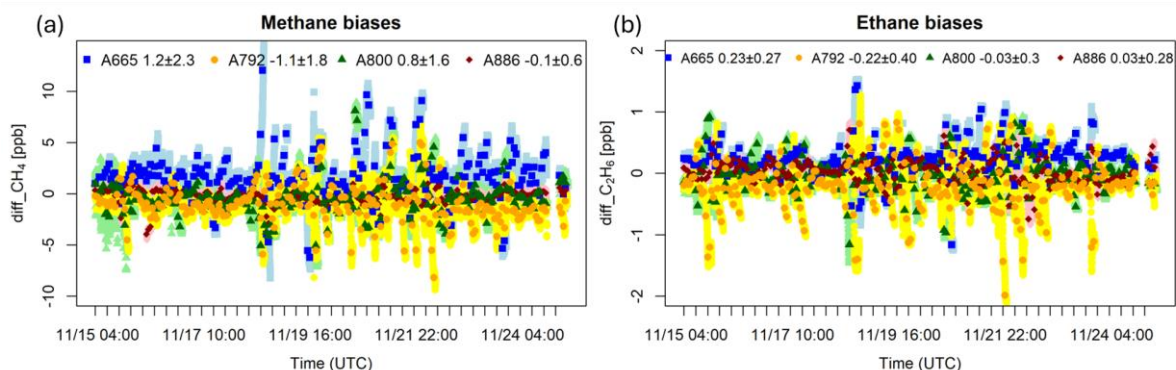
### 360 3.5 Total uncertainty

The mean estimated total uncertainty, including that due to errors in the water vapor correction, instrument noise between calibration cycles, and cylinder assignment error, during normal operations (hourly ambient cylinder calibration and nominal drying performance) is 0.8 - 3.0 ppb CH<sub>4</sub> and 0.35 - 0.37 ppb C<sub>2</sub>H<sub>6</sub>, depending on site, for hourly means. During longer times between calibration cycles or less effective drying, the uncertainty is higher, up to 6.1 ppb CH<sub>4</sub> and 0.46 ppb C<sub>2</sub>H<sub>6</sub>.

### 365 3.6 Comparisons (Tests 4 and 5)

#### 3.6.1 Concurrent laboratory tests (Test 4)

**Bias and standard deviation for hourly averages:** For the 10-day concurrent laboratory test, the mean biases for both methane (compared to the Picarro methane mole fraction) and ethane (compared to the mean ethane mole fraction derived from all Aeris instruments) (Fig. 7) are less than or equal to 1.2 ppb CH<sub>4</sub> and 0.23 ppb C<sub>2</sub>H<sub>6</sub> (specifically -1.1 to 1.2 ppb CH<sub>4</sub> and -0.22 to 0.23 ppb C<sub>2</sub>H<sub>6</sub>). The mean biases for methane and ethane were slightly worse, less than or equal to 1.9 ppb CH<sub>4</sub> and 0.24 ppb C<sub>2</sub>H<sub>6</sub>, for the original version (Version 1) over an 8-h concurrent test before the initial field deployment (not shown). When the averaging time for calibrated values is 1 h, the precision (standard deviations of the differences) is 0.6 to 2.3 ppb CH<sub>4</sub> and 0.20 to 0.40 ppb C<sub>2</sub>H<sub>6</sub> (Fig. 7, Version 2).



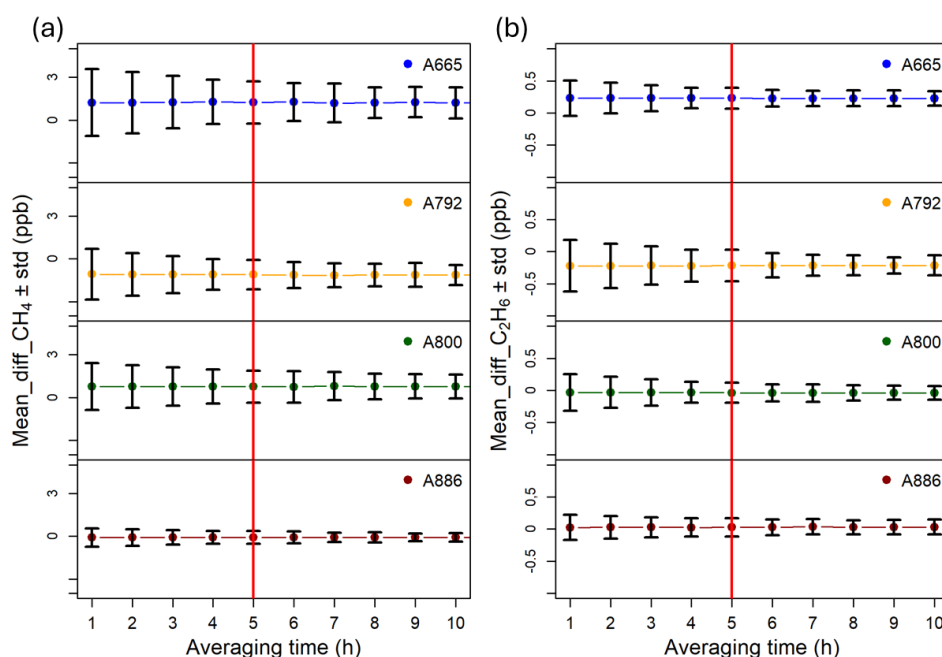
375 **Figure 7: The time series of the Aeris methane mole fractions (a) compared to the Picarro methane mole fraction, and Aeris ethane mole fractions (b) compared to the mean of the hourly ethane mole fraction from all Aeris sensors (Version 2) during the concurrent measurement laboratory test (15-25 November 2024). Light blue, yellow, light green and pink dots are the minute averaged data**



380 respectively for A665, A792, A800 and A886. Blue, orange, dark green and dark red dots are the hourly averaged data respectively for A665, A792, A800 and A886. The data were calibrated by running a full calibration cycle (i.e., both ambient and high cylinders) every 3 h. The numbers on the top represent the mean biases  $\pm$  standard deviation during the 10-day concurrent measurement test.

While the long-term bias and the standard deviations are within the estimated total uncertainty (0.8 - 3.0 ppb CH<sub>4</sub> and 0.35 - 0.37 ppb C<sub>2</sub>H<sub>6</sub>), the variability is higher than desired for some instruments, with individual hourly measurements with much higher errors (up to 11 ppb CH<sub>4</sub> and 2 ppb C<sub>2</sub>H<sub>6</sub>). These unrealistic deviations occur more frequently for serial numbers A665 and A792. Serial number A886 is the most stable instrument for both methane and ethane with the lowest standard deviation.

385 **Standard deviation as a function of averaging time:** The results considering the precision (standard deviation) as a function of averaging time for the concurrent laboratory tests (Fig. 8) show that as the averaging time increased, the deviations decreased, as is expected for instrument noise. For example, when the averaging time is 5 h, the standard deviations of the difference are 0.4 to 1.5 ppb CH<sub>4</sub> and 0.14 to 0.25 ppb C<sub>2</sub>H<sub>6</sub> (Fig. 8), depending on instrument.



390 **Figure 8:** The mean mole fraction differences (the same as those shown in Figure 8) and standard deviation as a function of averaging time for instrument serial numbers A665, A792, A800 and A886 respectively from top to bottom ((a) is for methane and (b) is for ethane). The blue, orange, dark green and dark red points represent the long-term mean bias for A665, A792, A800 and A886. The error bar represents the standard deviation of the shorter-term biases corresponding to the averaging time. The red lines represent an averaging time of 5 h.

395 **Testing of calibration approach:** Errors in the initial slope from the manufacturer were significant, but not as large as the offset error. Without applying any offset or slope adjustment using the Aeris software or in post-processing, the errors were up to 190 ppb CH<sub>4</sub> and 15 ppb C<sub>2</sub>H<sub>6</sub>, depending on the specific instrument. Without an initial full calibration cycle, i.e., using only the ambient cylinder with no slope adjustment from the manufacturer calibration, the mean bias increased to -3.2 to 4.9



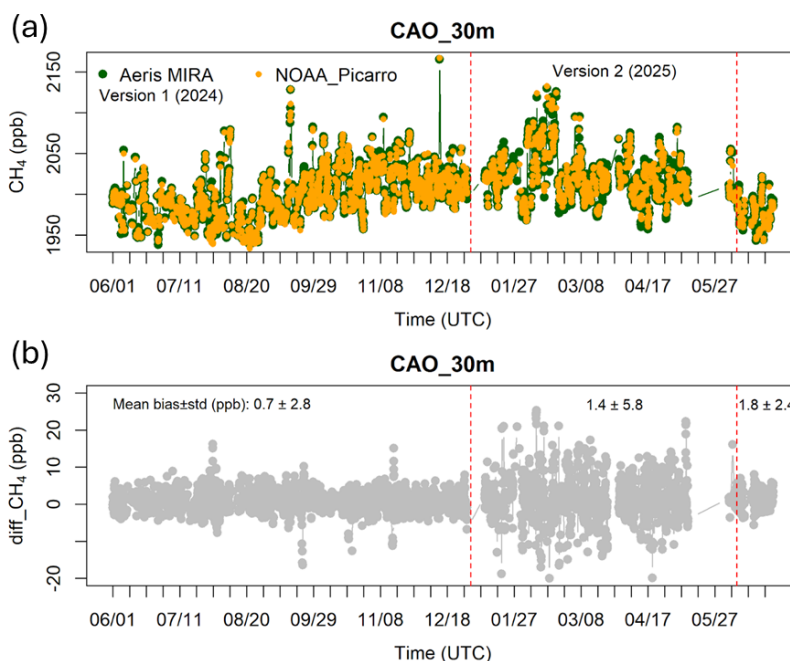
ppb CH<sub>4</sub> and -0.34 to 0.19 ppb C<sub>2</sub>H<sub>6</sub> and the standard deviation increased to 2.0 to 2.9 ppb CH<sub>4</sub> and 0.24 to 0.44 ppb C<sub>2</sub>H<sub>6</sub>,  
400 depending on instrument.

Use of an initial full calibration cycle and only the ambient cylinder offset calibrations every 3 h had little effect on the results compared to using full calibration cycles every 3 h, with mean biases changing by 0-0.4 ppb CH<sub>4</sub> and 0.01 - 0.02 ppb C<sub>2</sub>H<sub>6</sub> and standard deviation changing by less than 0.1 ppb CH<sub>4</sub> and less than 0.04 ppb C<sub>2</sub>H<sub>6</sub>. This result indicates that the slope of the true calibration curve does not change appreciably in a 10-day timeframe.

405 **Warm-up test:** We found no evidence for the need for a warm-up period for the Aeris instruments. When the power was lost for a short time (10 s), we found no effect on the instrument with no warm-up time needed for the warm restart. The cold start results showed that Aeris instruments reported no differences in the standard gases values before and after the instrument restarted and showed the instrument appeared to warm up quickly after restart. The first calibration cycles did not deviate from the subsequent cycles. The slope of the fit was not affected by outages ranging from a few seconds to 12 h during testing.

### 410 3.6.2 Field comparison (Test 5)

The differences between the NOAA Picarro CH<sub>4</sub> dry mole fraction and that of the collocated Aeris system differed primarily based on calibration frequency. The Aeris system showed a methane bias of 0.7 ppb CH<sub>4</sub>, with a standard deviation of the hourly differences of 2.8 ppb (Fig. 9) for Version 1 with calibrations every 3 h. The performance was considerably worse, with a mean methane difference of  $1.4 \pm 5.8$  ppb during the period when the ambient cylinder was sampled every 5 h (Fig. 9)  
415 (Version 2). After changing the calibration of the ambient cylinder from every 5 h to every 1 h, the methane differences were less noisy, with a mean bias of  $1.8 \pm 2.4$  ppb, for the version of the instrument and calibration scheme currently deployed in the field.



420 **Figure 9: (a) Calibrated hourly methane data from Aeris MIRA Ultra and NOAA Picarro at 30 m AGL at CAO over the time period**  
**of June 2024 - June 2025, and (b) the difference between Aeris MIRA Ultra and NOAA Picarro methane. The hours during which**  
**the Aeris' hourly standard deviation or NOAA Picarro's standard deviation was greater than the 50th percentile were not included**  
**(refer to Section 2.5.3). The first red dashed line represents the date on which the instrument was updated from Version 1 (with high**  
**and ambient cylinders sampled every 3 h) to Version 2 (with high cylinder sampled every 25 h and ambient cylinder every 5 h). The**  
 425 **second red dashed line represents the date on which the calibration period of the ambient cylinder was changed from every 5 h to**  
**every 1 h. The high cylinder was always sampled every 25 h for Version 2. The numbers on the top of (b) represent the mean bias ±**  
**standard deviation over the time periods divided by the red dashed lines. The data gaps were due to a software malfunction of the**  
**Aeris MIRA Ultra.**

#### 4 Discussion and conclusions

The Aeris MIRA Ultra instruments, with the modifications detailed in this paper, were able to achieve the compatibility goals  
 430 set for oil and gas regions. The compatibility (bias) indicated by the concurrent laboratory tests (better than 1.2 ppb CH<sub>4</sub> and  
 0.23 ppb C<sub>2</sub>H<sub>6</sub>) and by the field test at NOAA CAO (better than 1.8 ppb CH<sub>4</sub>) are within the target compatibility goals (3 ppb  
 CH<sub>4</sub> and 0.3 ppb C<sub>2</sub>H<sub>6</sub>) (Table 3). The laboratory and field test biases are less than the total uncertainty of the hourly calibrated  
 values (0.8 - 3.0 ppm CH<sub>4</sub> and 0.35 - 0.37 ppb C<sub>2</sub>H<sub>6</sub>), indicating consistency in the results. Instrument noise is the largest  
 component of uncertainty for C<sub>2</sub>H<sub>6</sub>, whereas water vapor uncertainty is the largest component for CH<sub>4</sub> (Table 3).

435 The precision (standard deviation) of the hourly calibrated values varied considerably among instruments (0.6 - 2.3 ppb CH<sub>4</sub>  
 and 0.20 - 0.40 ppb C<sub>2</sub>H<sub>6</sub> during concurrent laboratory tests; Section 3.6.1, Table 3). These results are consistent with the Allan  
 deviation analysis (Section 3.2), which indicated differing levels of instrument noise. Elevated noise in some instruments may  
 complicate interpretation for users relying on a single analyzer.



440 **Table 3: Summary of results under typical conditions (Version 2, hourly offset calibrations and full calibrations every 25 h, and typical drying). The compatibility (bias) goals are 3 ppb CH<sub>4</sub> and 0.3 ppb C<sub>2</sub>H<sub>6</sub>. Precision is the standard deviation of hourly calibrated differences. \*Instrument noise is also listed for 5-hourly (e.g., afternoon) means.**

Uncertainty	Typical magnitude (CH <sub>4</sub> )	Typical magnitude (C <sub>2</sub> H <sub>6</sub> )
Water vapor, U <sub>w</sub> <i>Bias</i>	0.6 - 3.0 ppb CH <sub>4</sub>	0.03 - 0.15 ppb C <sub>2</sub> H <sub>6</sub>
Instrument noise, U <sub>n</sub> <i>Noise</i>	0.74 ppb CH <sub>4</sub> (0.37 ppb CH <sub>4</sub> )*	0.25 ppb C <sub>2</sub> H <sub>6</sub> (0.11 ppb C <sub>2</sub> H <sub>6</sub> )*
Cylinder assignment, U <sub>c</sub> <i>Bias</i>	0.30 ppb CH <sub>4</sub>	0.12 ppb C <sub>2</sub> H <sub>6</sub>
Total, U <sub>t</sub> ( <i>bias and noise</i> )	0.8 - 3.0 ppb CH <sub>4</sub>	0.35 - 0.37 ppb C <sub>2</sub> H <sub>6</sub>
Difference of hourly calibrated values	Bias/Compatibility (Precision) (CH <sub>4</sub> )	Bias/Compatibility (Precision) (C <sub>2</sub> H <sub>6</sub> )
Test 4: Concurrent laboratory test	<= 1.2 ppb CH <sub>4</sub> (0.6 to 2.3 ppb CH <sub>4</sub> )	<= 0.23 ppb C <sub>2</sub> H <sub>6</sub> (0.20 to 0.40 ppb C <sub>2</sub> H <sub>6</sub> )
Test 5: Field test	1.8 ppb CH <sub>4</sub> (2.4 ppb CH <sub>4</sub> )	N/A

We determined the best calibration approach for our application, given practical limitations, to be a full calibration cycle (with ambient and high calibration cylinders) about once per day (every 25 h), with a more readily available ambient calibration cylinder sampled hourly. Without applying any zero or span using the Aeris software or in post-processing, the errors were up to 190 ppb CH<sub>4</sub> and 15 ppb C<sub>2</sub>H<sub>6</sub>, depending on the specific instrument. For applications requiring compatibility better than 3 ppb CH<sub>4</sub> and 0.3 ppb C<sub>2</sub>H<sub>6</sub>, it is essential to use at least one full calibration cycle (using two, or ideally more, cylinders) to correct for slope errors as the magnitude of the bias without adjusting the slope from the manufacturer calibration was up to 4.9 ppb CH<sub>4</sub> and 0.34 ppb C<sub>2</sub>H<sub>6</sub>. We performed a full calibration cycle every 25 h in the field as protection against potential slope changes in time. Using data from the high cylinders every 3 h instead of only once did not improve the instrument bias or precision in laboratory tests (Section 3.6.1). Calibrating less often (high cylinder every 25 h and ambient cylinder every 5 h) in the NOAA CAO field test did not significantly affect the bias but increased the standard deviation of hourly calibrated values from 2.4 to 5.8 ppm (Fig. 9, Section 3.6.2).

We observed substantial errors, defined as deviations from the reference instrument for CH<sub>4</sub> and from the mean for C<sub>2</sub>H<sub>6</sub>, the magnitude and frequency of which depended on the specific instrument (Fig. 7). These errors in hourly-averaged calibrated data were up to 11 ppb CH<sub>4</sub> and 2 ppb C<sub>2</sub>H<sub>6</sub> for serial numbers A665 and A792. For ethane, instrument noise poses a significant challenge because background concentrations at tower locations are typically only 0.5 - 1 ppb C<sub>2</sub>H<sub>6</sub>. Under these conditions, the noise can periodically result in unphysical negative hourly means, despite hourly calibrations. Since the perturbations are



caused by stochastic drift, their impact is reduced in magnitude by increasing the averaging time (Fig. 8). The perturbations  
460 may be particularly problematic for non-continuous applications with less data available to average, such as drone- and vehicle-  
based analyses.

The uncertainty due to instrument noise, which is larger compared to the target compatibility for ethane than for methane  
(Section 3.3, Table 3), can be further mitigated by considering longer averaging periods. The noise is reduced upon averaging,  
but not by the square root of the number of measurements as would be expected for random noise (Sections 3.3 and 3.6.1). For  
465 afternoon (5-hourly) means, with hourly calibrations using an ambient cylinder, the instrument noise uncertainty is quite low,  
0.37 ppb CH<sub>4</sub> (Fig. 5f) and 0.11 ppb C<sub>2</sub>H<sub>6</sub> (Fig. 6f).

For tower-based inversions with the goal of determining regional fluxes, site-specific long-term bias is more crucial than noise,  
and the primary potential sources of bias here are cylinder assignment error and uncertainty due to errors in the water vapor  
correction. Cylinder assignment error is low, 0.3 ppb CH<sub>4</sub> and 0.1 ppb C<sub>2</sub>H<sub>6</sub>, but any errors lead to a site-specific bias. Using  
470 more than two field cylinders at each site would likely reduce the effect of assignment error through averaging, and would  
allow for the ability to independently assess the uncertainty with a target cylinder.

The factory water correction for methane, and possibly for ethane, was not accurate enough for our purposes without partially  
removing this effect through calibration. Extrapolating the slopes for errors as a function of water vapor (Section 3.1) to a  
typical atmospheric value of 2%, the errors could be up to 130 ppb CH<sub>4</sub> and 6 ppb C<sub>2</sub>H<sub>6</sub> if the sample was not dried at all. We  
475 minimized the error by using a Nafion water exchanger to equilibrate the humidity between the sample and calibration gases,  
as is typically done in similar applications.

Even still, errors in the water correction likely lead to a site-specific bias that is difficult to disentangle given instrument noise  
and the temperature dependence of the Nafion dryer, and we recommend testing each instrument for water vapor response  
prior to deployment. We estimate that these biases due to water vapor correction range from 0.6 - 3.0 ppb CH<sub>4</sub> and 0.03 - 0.15  
480 ppb C<sub>2</sub>H<sub>6</sub> (Table 3, Section 3.1.2), for normal conditions, depending on the efficacy of the Nafion dryer and the ambient  
temperature of the building or shed as well as the manufacturer-supplied water vapor correction of each instrument. Because  
we only tested the water vapor response of four instruments, it is possible that there is a wider range of responses amongst  
instruments. Ideally the water vapor response would be tested multiple times and an instrument-specific water vapor correction  
applied, and repeated tests performed on a regular schedule as it is possible that the true water vapor correction of each  
485 instrument changes in time.

The impact of these biases on emissions quantification is dependent on the magnitude of the source being measured. For  
example, since the typical methane enhancements are above 60 to 200 ppb depending on season in the Permian basin (Monteiro  
et al., 2022) and above 40 ppb in the Denver-Julesburg Basin, a 3 ppb CH<sub>4</sub> bias due to an error in the water vapor correction  
will have minimal impact on the overall methane emissions calculation. However, the typical methane enhancements in the  
490 Indianapolis urban tower network are about 5 - 20 ppb, depending on the downwind tower (Miles et al., 2017). In this latter  
case, a 3 ppb bias in the instrument measurement can impact the downwind signal by up to 40%. Because emissions scale  
linearly with enhancements, this bias in the signal will impact the posterior emission calculation by a similar magnitude. The



495 Aeris MIRA Ultra system may not be a suitable instrument for coverage over regions with modest emission rates, unless the uncertainty is reduced by improving the drying stability between calibration and sample gas, or creating improved water vapor corrections. For regions with large signals, such as the Denver-Julesburg and Permian Basins, the uncertainty for the instrument design presented here is within an acceptable range.

The elaborate and time-consuming procedure used here to calibrate field cylinders for ethane was necessary because the Version 1 instruments lost their line lock after measuring dry air for an extended period of time (~20 min). This procedure is likely not needed for Version 2 with a software change allowing for line lock to occur using methane rather than water.

500 The Allan Deviation results presented here could be improved by separately testing for instrument noise and for water vapor dependence. We thus suggest cylinder tests both with and without an inline Nafion dryer/gas exchanger prior to deployment. The instrument noise is instrument specific and the uncertainty due to noise could be more accurately assessed, rather than using results from one of the instruments with higher noise as an upper bound, as was done here. It is also possible that the instrument noise is a function of mole fraction, either of the analyte, or of water vapor which is used for line locking. Improving  
505 the ambient temperature control or that of the cell may also improve the instrument noise performance. And finally the uncertainty could be significantly reduced by developing and applying instrument-specific water vapor corrections, if it can be determined that the function changes slowly enough for this approach to be practical.

The long-term reliability of these instruments in the field is a concern. Problems causing data loss to date include: malfunctioning of the thermoelectric cooler, failure of the sensor boards, inexplicable calibration shifts, solenoid valve or  
510 board failure, and unstable serial communication. Some of these issues were solved by power cycling the instruments remotely, but others necessitated physical intervention in the field, in the laboratory, or at the manufacturer.

In conclusion, the tower-based Aeris MIRA Ultra measurement system demonstrated in this study can provide stable and accurate data when carefully configured prior to deployment. The system shows promise for distinguishing among multiple methane emission sources by providing continuous ethane measurements, depending on the magnitudes of methane and ethane  
515 emissions. This capability is particularly valuable in regions such as the Denver–Julesburg Basin, where mixed thermogenic and biogenic methane sources complicate source attribution. More broadly, these instruments can advance our understanding of methane sources and improve our ability to disaggregate greenhouse gas emissions—an essential step toward informing effective mitigation strategies and addressing the climate crisis.

*Data availability.* The field data presented in this study are available at the following link: <https://doi.org/10.26208/RA58-SX41>. The citation is Liu, Y., N. L. Miles, S. J. Richardson, D. O. Miller, and B. J. Haupt. “Denver-Julesburg Basin: in-Situ  
520



Tower Greenhouse Gas Data.” Penn State Data Commons, 2025. <https://doi.org/10.26208/RA58-SX41>. The laboratory test data are available upon request.

*Author Contributions.* YL contributed to the lab experiments, data collection, data analysis, and writing of the paper. NLM and SJR contributed to the lab experiments’ design and setup, field deployment, project advising, reviewing, and editing the paper. DM contributed to building the auxiliary box, lab experiments, system integration, field deployment, and data collection. ZB contributed to reviewing and editing the paper. JK and PH contributed the NOAA Picarro measurements and data collection, and to reviewing and editing the paper. SD contributed to the quantification of the ethane calibration cylinders used for the laboratory tests and field measurements, and reviewing the paper. KJD, ZB, NLM and SJR conceptualized the field project. KJD contributed to project advising, reviewing, and editing the paper.

530 *Competing Interests.* The authors declare that they have no conflict of interest

*Acknowledgements.* We also would like to thank John Mund from NOAA GML for providing results of NOAA’s Round Robin Comparison Experiment used to determine the methane uncertainty of our calibration cylinders and thank Aeris technicians for their support and remote help. This study is based upon work supported by the Department of Energy under award DEFE0032288, and the NOAA Cooperative Agreement with CIRES, NA17OAR4320101.

535 *Financial support.* This research has been supported by the Department of Energy under award DEFE0032288, and the NOAA Cooperative Agreement with CIRES, NA17OAR4320101.

## References

- Allan, D. W.: Time and Frequency (Time-Domain) Characterization, Estimation, and Prediction of Precision Clocks and Oscillators, *IEEE Trans. Ultrason., Ferroelect., Freq. Contr.*, 34, 647–654, <https://doi.org/10.1109/T-UFFC.1987.26997>, 1987.
- 540 Alvarez, R. A., Zavala-Araiza, D., Lyon, D. R., Allen, D. T., Barkley, Z. R., Brandt, A. R., Davis, K. J., Herndon, S. C., Jacob, D. J., Karion, A., Kort, E. A., Lamb, B. K., Lauvaux, T., Maasackers, J. D., Marchese, A. J., Omara, M., Pacala, S. W., Peischl, J., Robinson, A. L., Shepson, P. B., Sweeney, C., Townsend-Small, A., Wofsy, S. C., and Hamburg, S. P.: Assessment of methane emissions from the U.S. oil and gas supply chain, *Science*, 361, 186–188, <https://doi.org/10.1126/science.aar7204>, 2018.
- 545 Andrews, A. E., Kofler, J. D., Trudeau, M. E., Williams, J. C., Neff, D. H., Masarie, K. A., Chao, D. Y., Kitzis, D. R., Novelli, P. C., Zhao, C. L., Dlugokencky, E. J., Lang, P. M., Crotwell, M. J., Fischer, M. L., Parker, M. J., Lee, J. T., Baumann, D. D.,



- Desai, A. R., Stanier, C. O., De Wekker, S. F. J., Wolfe, D. E., Munger, J. W., and Tans, P. P.: CO<sub>2</sub>, CO, and CH<sub>4</sub> measurements from tall towers in the NOAA Earth System Research Laboratory's Global Greenhouse Gas Reference Network: instrumentation, uncertainty analysis, and recommendations for future high-accuracy greenhouse gas monitoring efforts, *Atmos. Meas. Tech.*, 7, 647–687, <https://doi.org/10.5194/amt-7-647-2014>, 2014.
- 550 Barkley, Z., Davis, K., Miles, N., Richardson, S., Deng, A., Hmiel, B., Lyon, D., and Lauvaux, T.: Quantification of oil and gas methane emissions in the Delaware and Marcellus basins using a network of continuous tower-based measurements, *Atmospheric Chemistry and Physics*, 23, 6127–6144, <https://doi.org/10.5194/acp-23-6127-2023>, 2023.
- Barkley, Z. R., Lauvaux, T., Davis, K. J., Deng, A., Fried, A., Weibring, P., Richter, D., Walega, J. G., DiGangi, J., Ehrman, S. H., Ren, X., and Dickerson, R. R.: Estimating Methane Emissions From Underground Coal and Natural Gas Production in Southwestern Pennsylvania, *Geophysical Research Letters*, 46, 4531–4540, <https://doi.org/10.1029/2019GL082131>, 2019.
- 555 Barkley, Z. R., Davis, K. J., Feng, S., Cui, Y. Y., Fried, A., Weibring, P., Richter, D., Walega, J. G., Miller, S. M., Eckl, M., Roiger, A., Fiehn, A., and Kostinek, J.: Analysis of Oil and Gas Ethane and Methane Emissions in the Southcentral and Eastern United States Using Four Seasons of Continuous Aircraft Ethane Measurements, *JGR Atmospheres*, 126, e2020JD034194, <https://doi.org/10.1029/2020JD034194>, 2021.
- 560 Caulton, D. R., Li, Q., Bou-Zeid, E., Fitts, J. P., Golston, L. M., Pan, D., Lu, J., Lane, H. M., Buchholz, B., Guo, X., McSperritt, J., Wendt, L., and Zondlo, M. A.: Quantifying uncertainties from mobile-laboratory-derived emissions of well pads using inverse Gaussian methods, *Atmospheric Chemistry and Physics*, 18, 15145–15168, <https://doi.org/10.5194/acp-18-15145-2018>, 2018.
- 565 Collins, W., Orbach, R., Bailey, M., Biraud, S., Coddington, I., DiCarlo, D., Peischl, J., Radhakrishnan, A., and Schimel, D.: Monitoring methane emissions from oil and gas operations †, *Opt. Express*, 30, 24326, <https://doi.org/10.1364/OE.464421>, 2022.
- Commane, R., Hallward-Driemeier, A., and Murray, L. T.: Intercomparison of commercial analyzers for atmospheric ethane and methane observations, *Atmos. Meas. Tech.*, 16, 1431–1441, <https://doi.org/10.5194/amt-16-1431-2023>, 2023.
- 570 Defratyka, S. M., Paris, J.-D., Yver-Kwok, C., Loeb, D., France, J., Helmore, J., Yarrow, N., Gros, V., and Bousquet, P.: Ethane measurement by Picarro CRDS G2201-i in laboratory and field conditions: potential and limitations, *Atmospheric Measurement Techniques*, 14, 5049–5069, <https://doi.org/10.5194/amt-14-5049-2021>, 2021a.
- Defratyka, S. M., Paris, J.-D., Yver-Kwok, C., Fernandez, J. M., Korben, P., and Bousquet, P.: Mapping Urban Methane Sources in Paris, France, *Environ. Sci. Technol.*, 55, 8583–8591, <https://doi.org/10.1021/acs.est.1c00859>, 2021b.
- 575 Filges, A., Gerbig, C., Chen, H., Franke, H., Klaus, C., and Jordan, A.: The IAGOS-core greenhouse gas package: a measurement system for continuous airborne observations of CO<sub>2</sub>, CH<sub>4</sub>, H<sub>2</sub>O and CO, *Tellus B: Chemical and Physical Meteorology*, 67, 27989, <https://doi.org/10.3402/tellusb.v67.27989>, 2015.
- GAW Report No. 292: 21st WMO/IAEA Meeting on Carbon Dioxide, Other Greenhouse Gases and Related Tracers Measurement Techniques (GGMT-2022), Wageningen, The Netherlands, September 2022.



- 580 Karion, A., Sweeney, C., Kort, E. A., Shepson, P. B., Brewer, A., Cambaliza, M., Conley, S. A., Davis, K., Deng, A., Hardesty, M., Herndon, S. C., Lauvaux, T., Lavoie, T., Lyon, D., Newberger, T., Pétron, G., Rella, C., Smith, M., Wolter, S., Yacovitch, T. I., and Tans, P.: Aircraft-Based Estimate of Total Methane Emissions from the Barnett Shale Region, *Environ. Sci. Technol.*, 49, 8124–8131, <https://doi.org/10.1021/acs.est.5b00217>, 2015.
- Miles, N. L., Richardson, S. J., Lauvaux, T., Davis, K. J., Balashov, N. V., Deng, A., Turnbull, J. C., Sweeney, C., Gurney, K. R., Patarasuk, R., Razlivanov, I., Cambaliza, M. O. L., and Shepson, P. B.: Quantification of urban atmospheric boundary layer greenhouse gas dry mole fraction enhancements in the dormant season: Results from the Indianapolis Flux Experiment (INFLUX), *Elementa: Science of the Anthropocene*, 5, <https://doi.org/10.1525/elementa.127>, 2017.
- 585 Monteiro, V. C., Miles, N. L., Richardson, S. J., Barkley, Z., Haupt, B. J., Lyon, D., Hmiel, B., and Davis, K. J.: Methane, carbon dioxide, hydrogen sulfide, and isotopic ratios of methane observations from the Permian Basin tower network, *Earth System Science Data*, 14, 2401–2417, <https://doi.org/10.5194/essd-14-2401-2022>, 2022.
- 590 Myhre, G., Shindell, D., Bréon, F.-M., Collins, W., Fuglestedt, J., Huang, J., Koch, D., Lamarque, J.-F., Lee, D., Mendoza, B., Nakajima, T., Robock, A., Stephens, G., Zhang, H., Aamaas, B., Boucher, O., Dalsøren, S. B., Daniel, J. S., Forster, P., Granier, C., Haigh, J., Hodnebrog, Ø., Kaplan, J. O., Marston, G., Nielsen, C. J., O’Neill, B. C., Peters, G. P., Pongratz, J., Ramaswamy, V., Roth, R., Rotstayn, L., Smith, S. J., Stevenson, D., Vernier, J.-P., Wild, O., Young, P., Jacob, D., Ravishankara, A. R., and Shine, K.: 8 Anthropogenic and Natural Radiative Forcing, 2013.
- 595 Rella, C. W., Tsai, T. R., Botkin, C. G., Crosson, E. R., and Steele, D.: Measuring Emissions from Oil and Natural Gas Well Pads Using the Mobile Flux Plane Technique, *Environ. Sci. Technol.*, 49, 4742–4748, <https://doi.org/10.1021/acs.est.5b00099>, 2015.
- Richardson, S. J., Miles, N. L., Davis, K. J., Lauvaux, T., Martins, D. K., Turnbull, J. C., McKain, K., Sweeney, C., and Cambaliza, M. O. L.: Tower measurement network of in-situ CO<sub>2</sub>, CH<sub>4</sub>, and CO in support of the Indianapolis FLUX (INFLUX) Experiment, *Elementa: Science of the Anthropocene*, 5, 59, <https://doi.org/10.1525/elementa.140>, 2017.
- 600 Robertson, A. M., Edie, R., Snare, D., Soltis, J., Field, R. A., Burkhart, M. D., Bell, C. S., Zimmerle, D., and Murphy, S. M.: Variation in Methane Emission Rates from Well Pads in Four Oil and Gas Basins with Contrasting Production Volumes and Compositions, *Environ. Sci. Technol.*, 51, 8832–8840, <https://doi.org/10.1021/acs.est.7b00571>, 2017.
- 605 Roscioli, J. R., Yacovitch, T. I., Floerchinger, C., Mitchell, A. L., Tkacik, D. S., Subramanian, R., Martinez, D. M., Vaughn, T. L., Williams, L., Zimmerle, D., Robinson, A. L., Herndon, S. C., and Marchese, A. J.: Measurements of methane emissions from natural gas gathering facilities and processing plants: measurement methods, *Atmospheric Measurement Techniques*, 8, 2017–2035, <https://doi.org/10.5194/amt-8-2017-2015>, 2015.
- Saunio, M., Stavert, A. R., Poulter, B., Bousquet, P., Canadell, J. G., Jackson, R. B., Raymond, P. A., Dlugokencky, E. J., Houweling, S., Patra, P. K., Ciais, P., Arora, V. K., Bastviken, D., Bergamaschi, P., Blake, D. R., Brailsford, G., Bruhwiler, L., Carlson, K. M., Carrol, M., Castaldi, S., Chandra, N., Crevoisier, C., Crill, P. M., Covey, K., Curry, C. L., Etiope, G., Frankenberg, C., Gedney, N., Hegglin, M. I., Höglund-Isaksson, L., Hugelius, G., Ishizawa, M., Ito, A., Janssens-Maenhout, G., Jensen, K. M., Joos, F., Kleinen, T., Krummel, P. B., Langenfelds, R. L., Laruelle, G. G., Liu, L., Machida, T., Maksyutov,



- S., McDonald, K. C., McNorton, J., Miller, P. A., Melton, J. R., Morino, I., Müller, J., Murguia-Flores, F., Naik, V., Niwa, Y.,  
615 Noce, S., O'Doherty, S., Parker, R. J., Peng, C., Peng, S., Peters, G. P., Prigent, C., Prinn, R., Ramonet, M., Regnier, P., Riley,  
W. J., Rosentreter, J. A., Segers, A., Simpson, I. J., Shi, H., Smith, S. J., Steele, L. P., Thornton, B. F., Tian, H., Tohjima, Y.,  
Tubiello, F. N., Tsuruta, A., Viovy, N., Voulgarakis, A., Weber, T. S., van Weele, M., van der Werf, G. R., Weiss, R. F.,  
Worthy, D., Wunch, D., Yin, Y., Yoshida, Y., Zhang, W., Zhang, Z., Zhao, Y., Zheng, B., Zhu, Q., Zhu, Q., and Zhuang, Q.:  
The Global Methane Budget 2000–2017, *Earth System Science Data*, 12, 1561–1623, [https://doi.org/10.5194/essd-12-1561-](https://doi.org/10.5194/essd-12-1561-2020)  
620 2020, 2020.
- Schwietzke, S., Griffin, W. M., Matthews, H. S., and Bruhwiler, L. M. P.: Natural Gas Fugitive Emissions Rates Constrained  
by Global Atmospheric Methane and Ethane, *Environ. Sci. Technol.*, 48, 7714–7722, <https://doi.org/10.1021/es501204c>, 2014.
- Shah, A., Pitt, J., Kabbabe, K., and Allen, G.: Suitability of a Non-Dispersive Infrared Methane Sensor Package for Flux  
Quantification Using an Unmanned Aerial Vehicle, *Sensors*, 19, 4705, <https://doi.org/10.3390/s19214705>, 2019.
- 625 WMO Greenhouse Gas Bulletin (GHG Bulletin)-No.18: The State of Greenhouse Gases in the Atmosphere Based on Global  
Observations through 2021, WMO,  
<https://library.wmo.int/viewer/58743/?offset=#page=1&viewer=picture&o=bookmarks&n=0&q=> (last access: 25 November  
2024), 2022.
- Yver Kwok, C., Laurent, O., Guemri, A., Philippon, C., Wastine, B., Rella, C. W., Vuillemin, C., Truong, F., Delmotte, M.,  
630 Kazan, V., Darding, M., Lebègue, B., Kaiser, C., Xueref-Rémy, I., and Ramonet, M.: Comprehensive laboratory and field  
testing of cavity ring-down spectroscopy analyzers measuring H<sub>2</sub>O, CO<sub>2</sub>, CH<sub>4</sub> and CO, *Atmospheric Measurement Techniques*,  
8, 3867–3892, <https://doi.org/10.5194/amt-8-3867-2015>, 2015.